European Journal of Medicinal Chemistry 243 (2022) 114675

Contents lists available at ScienceDirect

European Journal of Medicinal Chemistry

journal homepage: www.elsevier.com/locate/ejmech

Research paper

Identification of L. *infantum* trypanothione synthetase inhibitors with leishmanicidal activity from a (non-biased) in-house chemical library

Mercedes Alcón-Calderón [a,1], Héctor de Lucio [a,**,1], Juan Carlos García-Soriano [a], Alejandro Revuelto [b], Sonia de Castro [b], Celia López-Gutiérrez [a], Ana San-Félix [b], Ernesto Quesada [b], Federico Gago [c,d], María-José Camarasa [b], Antonio Jiménez-Ruiz [a,d,***], Sonsoles Velázquez [b,*]

[a] Universidad de Alcalá, Departamento de Biología de Sistemas, 28805, Alcalá de Henares, Madrid, Spain
[b] Instituto de Química Médica (IQM, CSIC), Juan de la Cierva 3, 28006, Madrid, Spain
[c] Universidad de Alcalá, Área de Farmacología, Departamento de Ciencias Biomédicas, 28805, Alcalá de Henares, Madrid, Spain
[d] Laboratorio de Modelado Molecular, Unidad asociada al CSIC por el IQM, 28805, Alcalá de Henares, Madrid, Spain

ARTICLE INFO

Keywords:
Trypanothione synthetase
Leishmania infantum
Competitive and non-competitive inhibitors
Molecular docking
Molecular dynamics

ABSTRACT

Redox homeostasis in trypanosomatids is based on the low-molecular-weight trypanothione, an essential dithiol molecule that is synthetized by trypanothione synthetase (TryS) and maintained in its reduced state by trypanothione disulfide reductase (TryR). The fact that both enzymes are indispensable for parasite survival and absent in the mammalian hosts makes them ideal drug targets against leishmaniasis. Although many efforts have been directed to developing TryR inhibitors, much less attention has been focused on TryS. The screening of an in-house library of 144 diverse molecules using two parallel biochemical assays allowed us to detect 13 inhibitors of *L. infantum* TryS. Compounds **1** and **3** were characterized as competitive inhibitors with K_i values in the low micromolar range and plausible binding modes for them were identified by automated ligand docking against refined protein structures obtained through computational simulation of an entire catalytic cycle. The proposed binding site for both inhibitors overlaps the polyamine site in the enzyme and, additionally, **1** also occupies part of the ATP site. Compound **4** behaves as a mixed hyperbolic inhibitor with a K_i of 0.8 μM. The activity of **5** is clearly dependent on the concentration of the polyamine substrate, but its kinetic behavior is clearly not compatible with a competitive mode of inhibition. Analysis of the activity of the six best inhibitors against intracellular amastigotes identified **5** as the most potent leishmanicidal candidate, with an EC_{50} value of 0.6 μM and a selectivity index of 35.

1. Introduction

Leishmaniasis is a neglected tropical disease caused by protozoan parasites of the genus *Leishmania* [1]. This antropozoonotic disease is transmitted to humans and other mammalian hosts through the bite of infected female sandflies from different species of the genera *Phlebotomus* and *Lutzomyia* in the Old and New World, respectively [2]. *Leishmania* parasites exhibit a digenetic life cycle with two developmental forms: promastigotes, which are an extracellular motile form adapted to the sandfly vector, and amastigotes, which are intracellular non-motile forms adapted to the mammalian hosts [3,4]. Leishmaniasis manifests as different clinical syndromes among which cutaneous

Abbreviations: ALPs, alkyl-lysophospholipids; CL, cutaneous leishmaniasis; *Ec*GspS, *E. coli* GspdSH synthetase; GR, glutathione-disulfide reductase; GSH, glutathione; GspdSH, glutathionylspermidine; HepG2, human hepatocellular carcinoma cells; *Li*TryS, *L. infantum* TryS; *Lm*TryS, *L. major* TryS; MCL, mucocutaneous leishmaniasis; *Tb*TryS, *T. brucei* TryS; Trx, thioredoxin; TrxR, thioredoxin-disulfide reductase; TryS, trypanothione synthetase-amidase; TryR, trypanothione disulfide reductase; $T(SH)_2$, N^1,N^8-bis(glutathionyl)-spermidine; Spd, triamine spermidine; VL, visceral leishmaniasis; WHO, World Health Organization.

* Corresponding author.
** Corresponding author.
*** Corresponding author. Laboratorio de Modelado Molecular, Unidad asociada al CSIC por el IQM, 28805, Alcalá de Henares, Madrid, Spain.
E-mail addresses: hector.lucio@edu.uah.es (H. de Lucio), antonio.jimenez@uah.es (A. Jiménez-Ruiz), iqmsv29@iqm.csic.es (S. Velázquez).
[1] These two authors contributed equally to this work.

https://doi.org/10.1016/j.ejmech.2022.114675
Received 30 June 2022; Received in revised form 5 August 2022; Accepted 8 August 2022
Available online 18 August 2022

leishmaniasis (CL), mucocutaneous leishmaniasis (MCL) and visceral leishmaniasis (VL) are the most prevalent. VL, also known as kala-azar, is lethal in over 95% of cases if left untreated [1]. This form of the disease is characterized by the dissemination of its etiological agents, namely *Leishmania donovani* and *Leishmania infantum* parasites, to distant tissues such as the liver, spleen, and bone marrow [5,6].

According to the World Health Organization (WHO), the estimated incidence of leishmaniasis is 700,000 to 1 million new cases per year and one billion people live in endemic areas of leishmaniasis with a high risk of infection [1,7,8]. VL is the second deadliest parasitic disease after malaria, with more than 600 million people at risk of infection and an estimated incidence of 50,000–90,000 new cases per year [1,6,9]. Unfortunately, there is not yet any licensed vaccine for humans and the current chemotherapeutic arsenal for the treatment of leishmaniasis is still unsatisfactory due to important drawbacks, specifically high toxicity, poor efficacy, prohibitive costs, and appearance of drug resistances [8,10,11]. Considering the limitations mentioned, research in drug discovery for the treatment of leishmaniasis is imperative. Besides the usual problems related to activity and specificity, development of innovative, effective, and less toxic leishmanicidal drugs is highly challenging because three different layers of cell membranes (plasma membrane of the host cell, phagolysosome membrane, and plasma membrane of the parasite) must be crossed before any molecule can selectively kill *Leishmania* intracellular amastigotes.

Metabolic pathways that are both indispensable for parasite survival and absent from their respective mammalian hosts are considered ideal targets for screening campaigns in target-based drug discovery efforts against protozoan parasitic diseases [12,13]. In this regard, all members of the Trypanosomatidae family, to which *Leishmania* parasites belong, lack the canonical eukaryotic systems for maintaining the intracellular thiol-redox homeostasis, namely glutathione/glutathione-disulfide reductase (GSH/GR) and thioredoxin/thioredoxin-disulfide reductase (Trx/TrxR). Instead, trypanosomatids maintain their redox homeostasis due to their unique thiol metabolism, which is based on the low-molecular-weight dithiol trypanothione [N^1,N^8-bis(glutathionyl)-spermidine; $T(SH)_2$] and trypanothione-disulfide reductase (TryR), which is an NADPH-dependent oxidoreductase responsible for keeping trypanothione in its reduced form. $T(SH)_2$ is the central molecule in the thiol metabolism of trypanosomatids as it delivers reducing equivalents, directly or through thioredoxin-like proteins termed tryparedoxins, to effector proteins involved in essential processes such as initiation of kinetoplast DNA minicircles replication, synthesis of precursors for DNA replication, and detoxification of ketoaldehydes, hydroperoxides and metal-containing drugs [14]. Many efforts have been focused on the screening, design, and evaluation of TryR inhibitors, as indicated by the more than five hundred published articles that deal with this enzyme as a drug target. In contrast, trypanothione synthetase-amidase (TryS), the enzyme that catalyzes the final step in the $T(SH)_2$ biosynthetic pathway, has received much less attention as a target. TryS is a bifunctional enzyme comprising two structurally distinct domains that are responsible for its two conflicting biosynthetic and hydrolytic activities [13–15]. Through its C-terminal ATP-dependent C–N ligase domain, TryS catalyzes the stepwise covalent conjugation of two GSH molecules onto the triamine spermidine (Spd). In the first reaction, TryS catalyzes the formation of an amide bond between the glycine's carboxyl group of the first GSH molecule, which is previously activated by phosphorylation at the expense of one ATP molecule, and the free N^1 or N^8 amino groups of spermidine to give N^1- or N^8-glutathionylspermidine (GspdSH), respectively. In the second reaction, N^1- or N^8-GspdSH is subsequently conjugated to the second GSH molecule at the expense of another ATP molecule to give $T(SH)_2$ [12–15]. The essential role of TryS in the survival of *Trypanosoma brucei* and *L. infantum* was clearly established from experiments demonstrating that generation of null mutants of the gene encoding TryS could only be accomplished upon simultaneous episomal expression of TryS [13,16]. TryS has also been chemically validated as a drug target, since on-target inhibitors of TryS, such as the phenyl-indazoles DDD86243 and DDU86439, were identified in a high-throughput screen of 63,362 compounds against *T. brucei* TryS (*Tb*TryS) [12,13].

Most of the reported TryS inhibitors show a competitive mode of inhibition against the polyamine substrate (either Spd or GspdSH) [12, 17–19] and only a few exceptions have been identified, namely the oxabicyclo[3.3.1]nonanone PS-203, as GSH competitors [20]. Ebselen and the natural sesquiterpene lactone cynaropicrin were both described as irreversible inhibitors [21,22].

We herein describe the results of a screening campaign that tested an in-house library of 144 diverse compounds from the Medicinal Chemistry Institute of the Spanish Research Council using L. *infantum* TryS (*Li*TryS) as the molecular target. The library contains a collection of complex and diverse molecules that encompass a variety of molecular skeletons and covers a wide area of chemical space. Synthesis of these molecules was not biased towards *Li*TryS as a pre-defined biological target. We consider that this structural diversity is a useful strategy to identify lead compounds that may be further improved by target-oriented synthesis after detailed inspection of their interactions with the enzyme. In addition to the well-established TryS ligase activity assay based on phosphate quantification with BIOMOL Green reagent [12,17], all compounds were also tested using a newly developed assay in which TryS ligase and TryR activities are coupled for detection of the produced $T(SH)_2$. 13 compounds were identified as *Li*TryS inhibitors in both biochemical assays and their inhibition mechanism was elucidated through *in vitro* kinetic characterization. The leishmanicidal activity of 6 selected molecules was also analyzed. Finally, computational studies allowed us to provide mechanistic details of the ligase activity of TryS and to identify the putative binding sites of the selected compounds.

2. Results and discussion

2.1. Identification of LiTryS inhibitors

The different steps of the screening workflow are shown on Fig. 1. In the first step, all compounds were tested using two different biochemical assays that measured *Li*TryS ligase activity by quantifying either the inorganic phosphate formed in the reaction using the BIOMOL Green reagent or the thiol-containing products GspdSH and/or $T(SH)_2$ using a DTNB/*Li*TryR-coupled assay. *Li*TryS enzymatic reactions were performed with saturating and near physiological concentrations of all the substrates. Concentrations of the enzyme and the substrates, as well as the reaction volume, were adjusted to be exactly the same in both biochemical assays, allowing, if desired, simultaneous determination of the inhibitory capacity of the molecules in both enzymatic reactions.

Compounds were tested once in each biochemical assay at a single point concentration of 25 μM. For practical reasons, screenings performed with each activity assay were subdivided into two sets of 72 compounds, thus 4 independent assays were performed. The quality of the biochemical assays used in this primary screening was assessed in terms of robustness and reproducibility using various criteria. The average Z' factor for the two screening sets performed with the standard BIOMOL Green assay was 0.78 ± 0.04, while for the two screening sets performed with the DTNB/*Li*TryR-coupled assay was 0.79 ± 0.005. The average signal-to-background values were 3.45 ± 0.44 and 2.57 ± 0.35 for the two screening sets performed with the standard BIOMOL Green and the DTNB/*Li*TryR-coupled assays, respectively. Notably, an excellent correlation for the data obtained in both assays was revealed by the highly significant Pearson coefficient (0.92) (Fig. 2). Compounds rendering inhibition rates ≥50% in both biochemical assays were designated as primary hits. As shown in Fig. 2 (grey square), thirteen compounds fulfilled this criterion and were identified as *Li*TryS inhibitors.

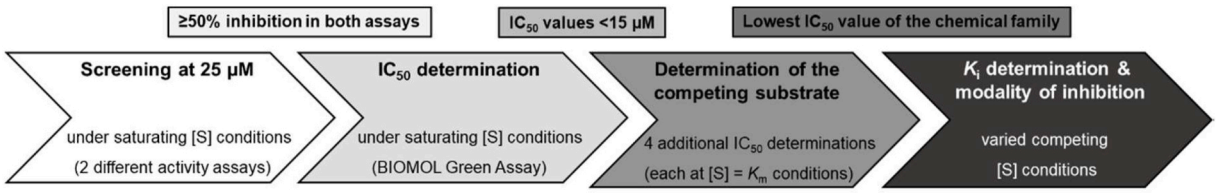

Fig. 1. Schematic workflow for the screening campaign. The different phases, the most relevant conditions of the biochemical assays and the selection criteria are shown in boxes.

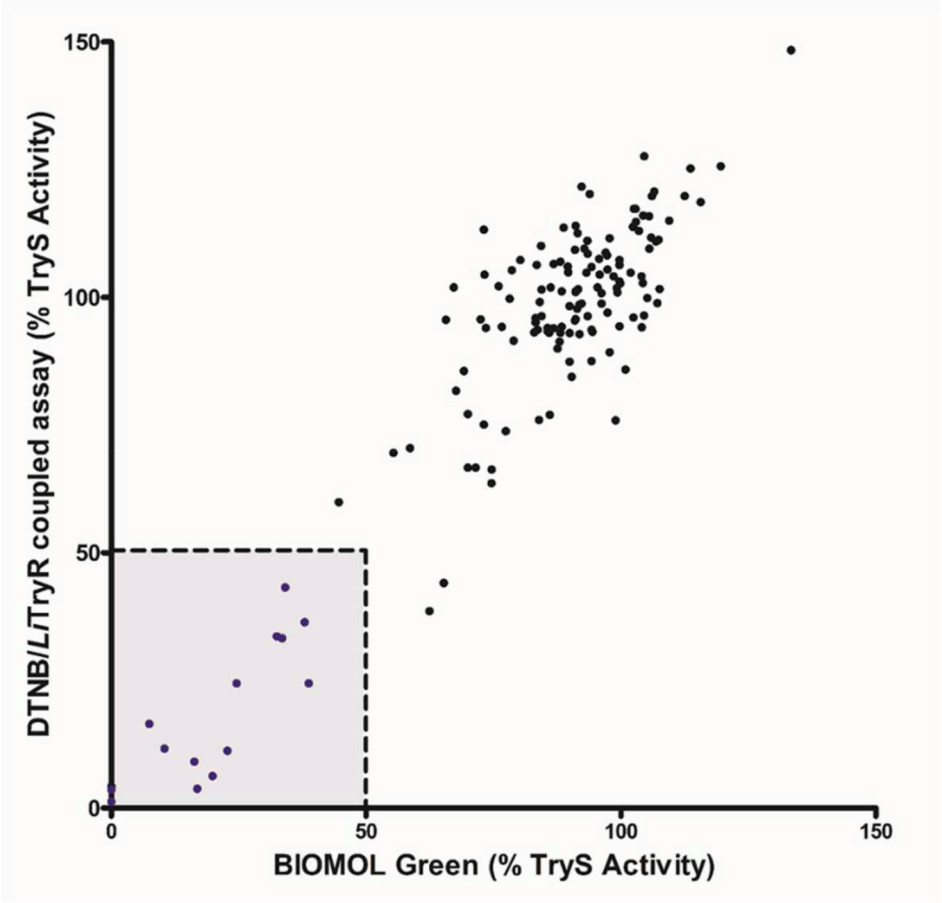

Fig. 2. *Li*TryS hit discovery campaign. An in-house chemical library of 144 compounds was tested at 25 μM for their inhibitory activity against *Li*TryS using two different biochemical assays: the standard BIOMOL Green assay and the DTNB/*Li*TryR-coupled assay. Data points shown in the graph represent the remaining *Li*TryS activity (%) due to compound inhibition. Linear regression of these data returned a Pearson correlation coefficient (r) of 0.92 and a coefficient of determination (R^2) of 0.85. Results were obtained in 4 independent experiments corresponding to 2 sets of 72 compounds, each of them carried out with both *Li*TryS activity assays.

2.2. Characterization of selected LiTryS inhibitors

The thirteen selected compounds were further analyzed to obtain their IC_{50} values under saturating concentrations of all three substrates (ATP, GSH and Spd). As shown in Table 1 (Saturating [S]), the IC_{50} values obtained in these dose-response experiments ranged from 4.4 to 23.7 μM. The six compounds displaying IC_{50} values below 15 μM were considered promising *Li*TryS inhibitors and were subsequently assayed at reduced concentrations of each substrate. The aim of this third step was to ascertain whether they could compete with any of the *Li*TryS substrates for their binding site at the free enzyme. Thus, three additional IC_{50} values were determined under the slightly altered assay conditions generated after individually reducing every substrate concentration to its K_m value in the *Li*TryS-catalyzed reaction (abbreviated as [ATP], [GSH] or [Spd] = K_m conditions). Because the K_m value for GspdSH was much smaller than that obtained for Spd, we were also interested in evaluating the putative competitive behavior of the inhibitors for this substrate. Accordingly, the activity of the selected inhibitors was also tested at saturating concentrations of ATP, GSH and GspdSH and compared to their activity at a GspdSH concentration equivalent to its K_m (Table 1 last two columns). As expected, most of the IC_{50} values calculated under non-saturating substrate concentrations differed from those calculated initially (Table 1). Indeed, except for **2** and **4**, all compounds clearly increased their inhibitory activity when the concentration of the polyamine substrate (either Spd or GspdSH) was reduced. Accordingly, **2** and **4** show a noncompetitive behavior with respect to all the substrates, which apparently excludes them from the enzyme's active site. On the contrary, the finding that binding of **1**, **3**, **5**, and **6** is affected by the presence of high concentrations of either Spd or GspdSH is compatible with a competitive mode of inhibition and suggests that the putative binding site of these compounds may overlap with the polyamine binding site in *Li*TryS. Changes in the activity of the inhibitors in the presence of high ATP concentrations were only observed for **1,** whose binding site could also be ascribed to the ATP pocket.

The chemical structures of compounds **1**–**6** are shown in Fig. 3. The hit set contained molecules from three distinct structural classes: triazole-phenyl-thiazoles (**1**) [23], polyphenol-carbohydrate hybrids (**2**

Table 1
Activity of compounds selected from the screen against *Li*TryS.

Compound	IC_{50} values (μM)[a]					
	Spd as polyamine S				GspdSH as polyamine S	
	Saturating [S]	[ATP] = K_m[b]	[GSH] = K_m[b]	[Spd] = K_m[b]	Saturating [S]	[GspdSH] = K_m[b]
1	14.8 ± 0.4	8.7 ± 0.2	14.2 ± 1.9	10.9 ± 1.1	16.2 ± 2.4	10.7 ± 0.7
2	5.4 ± 0.6	7.1 ± 1.1	6.7 ± 1.1	4.7 ± 0.4	5.9 ± 0.3	5.1 ± 1.4
3	14.8 ± 0.6	13.4 ± 0.4	14.6 ± 0.3	9.9 ± 0.1	7.2 ± 0.1	4.9 ± 0.02
4	4.4 ± 0.7	5.4 ± 1.5	5.4 ± 1.2	5.6 ± 1.0	2.2 ± 0.5	2.0 ± 0.6
5	7.9 ± 1.1	7.3 ± 0.3	7.8 ± 0.4	5.5 ± 0.4	7.1 ± 0.2	3.8 ± 1.0
6	9.8 ± 1.0	8.9 ± 0.7	8.7 ± 0.9	8.4 ± 0.4	7.5 ± 0.2	6.0 ± 0.1
7	15.9 ± 3.2	–	–	–		–
8	21.7 ± 2.3	–	–	–		–
9	17.4 ± 1.0	–	–	–		–
10	21.2 ± 1.5	–	–	–		–
11	20.1 ± 0.6	–	–	–		–
12	17.6 ± 2.6	–	–	–		–
13	23.7 ± 0.4	–	–	–		–

[a] Half-maximal inhibitory concentration (IC_{50}) ± standard error (SE) values for selected compounds in the *Li*TryS activity assay using the BIOMOL Green reagent. Results are representative of three independent experiments.

[b] IC_{50} values were determined with the specified substrate at the respective K_m value of *Li*TryS while maintaining the other substrates under saturating concentrations.

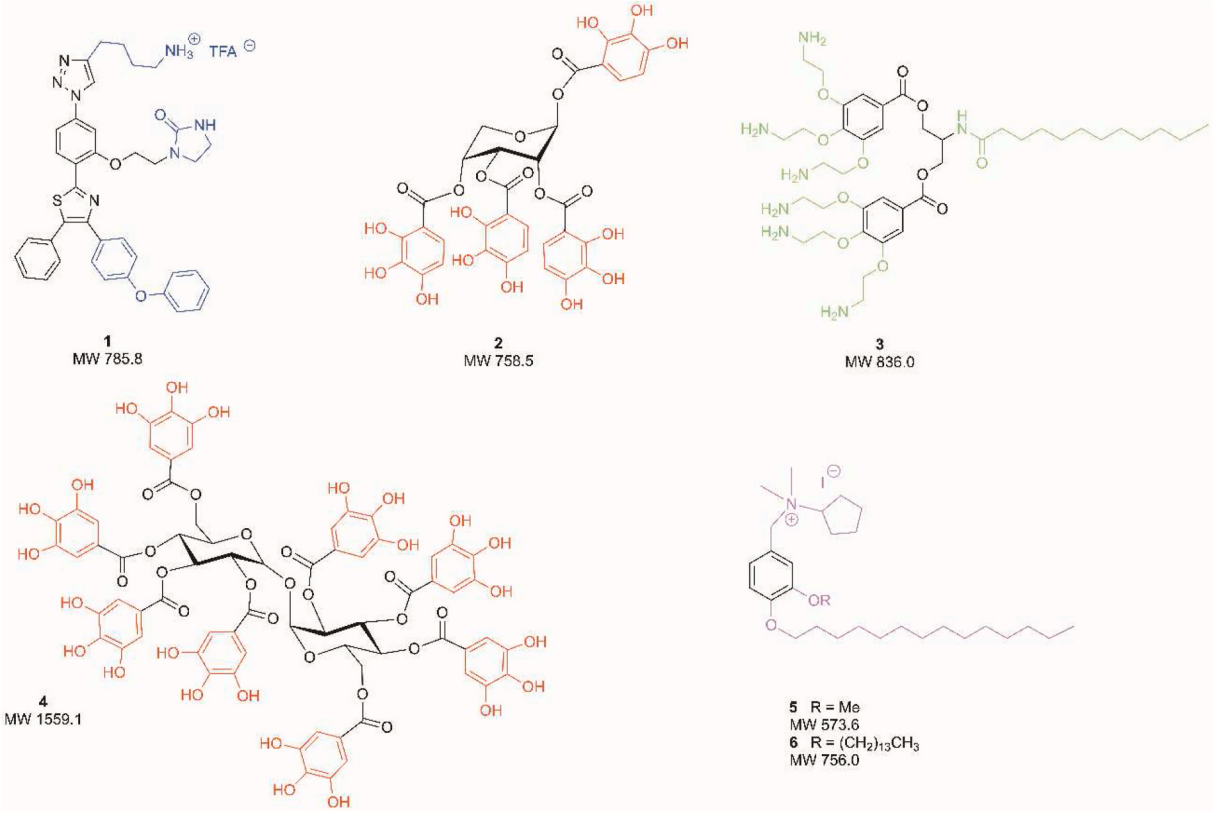

Fig. 3. Chemical structure and molecular weight of the most relevant *Li*TryS hits from the in-house library of 144 compounds. The moieties of interest are highlighted in different colors.

and **4**) [24], and amphiphiles with polyamino (**3**) [25] or benzylammonium polar heads (**5** and **6**) [26] attached to long aliphatic tails. The synthesis and characterization of novel compound **5** (see Scheme S1) together with the analytical and spectroscopic data of the hits **1**–**4** are fully described in the Supplementary Material.

Given the similarities between **2** and **4**, on the one hand, and **5** and **6**, on the other hand, and because of the higher IC_{50} values obtained for **2** and **6**, these two compounds were discarded for the final stage of the screening campaign. Consequently, the concentrations of both inhibitor and substrate were changed to define the K_i values and modalities of inhibition only for compounds **1**, **3**, **4** and **5**.

The strong decrease in the IC_{50} value obtained for **1** at a reduced concentration of ATP prompted us to evaluate its behavior under different concentrations of this substrate. The results shown in Fig. 4A corroborate a competitive mode of inhibition for **1** against ATP and allowed us to estimate a K_i value of 5.4 ± 1.2 μM. A significant reduction in the IC_{50} values was also observed for this compound when the concentration of either Spd or GspdSH was reduced to their K_m values. When Spd is used as the substrate, TryS catalyzes both the transformation of Spd to GspdSH and that of GspdSH to $T(SH)_2$. Thus, in fact,

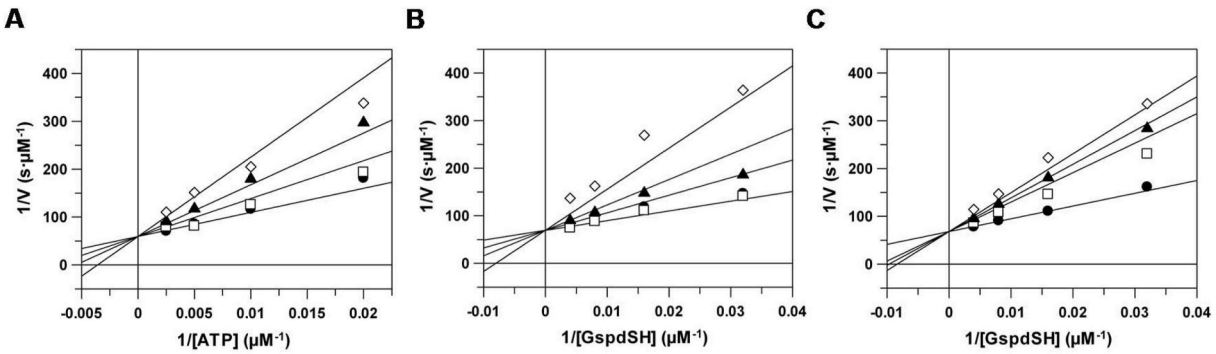

Fig. 4. Competitive inhibition of *Li*TryS by hits **1** and **3**. Lineweaver-Burk double-reciprocal plots plot of the initial velocity of the *Li*TryS ligase reaction as a function of the ATP (**A**) and GspdSH (**B**) concentrations measured at different concentrations of **1**: 0 μM (●), 3.1 μM (□), 6.2 μM (▲) and 12.5 μM (◇). (**C**) Lineweaver-Burk double-reciprocal plots plot of the initial velocity of *Li*TryS ligase reaction as a function of the GspdSH concentration measured at different concentrations of **3**: 0 μM (●), 3.3 μM (□), 4.2 μM (▲) and 5.2 μM (◇). Lines shown in the plots were obtained by fitting the reciprocal data to Equation (4). Results are representative of three independent experiments.

two different substrates with different K_m values (both binding to the same site in the enzyme) are analyzed simultaneously. A precise kinetic analysis is not feasible under this complex situation and, consequently, the simple reaction that transforms GspdSH to $T(SH)_2$ was used for this analysis. A K_i value of 3.9 ± 1.6 μM and a competitive mode of inhibition was also observed against GspdSH (Fig. 4B).

The inhibitory activity of **3** is also strongly enhanced at reduced concentrations of both Spd and GspdSH. A kinetic analysis at different concentrations of **3** and GspdSH confirmed a competitive mode of inhibition against this substrate and revealed a *Ki* value of 2.6 ± 0.5 μM (Fig. 4C).

The finding that the inhibitory activity of **4** does not increase upon reduction of the concentration of any of the *Li*TryS substrates (Table 1) discards a competitive mode of inhibition. However, the experimental data obtained could be fitted neither to a classical noncompetitive nor to a classical mixed inhibition modality. According to the results shown in Fig. 5B, this compound shows a K_i value of 0.8 ± 0.2 μM and displays a mixed (α = 1.2 ± 0.4) hyperbolic (β = 0.3 ± 0.04) inhibition of *Li*TryS when assayed against different concentrations of GspdSH. The α value obtained clearly excludes a competitive mode of inhibition and indicates the formation of a complex (ESI complex) that includes the enzyme (E), the substrate (S), and the inhibitor (I). A β value of 0.3 indicates that this ESI complex is still able to catalyze the reaction at 30% of the velocity of the uninhibited enzyme (Fig. 5A)

The inhibitory activity of **5** is also clearly influenced by the concentration of the polyamine substrate in the TryS ligase reaction. Apparent K_m and V_{max} values could be obtained for every concentration of inhibitor assayed at varying concentrations of GspdSH (see Fig. S2 and Table S1 in the Supplementary data) but the whole set of experimental data points could not be fitted to any of the modes of inhibition tested. The progressive decrease in the V_{max} values observed upon increasing concentrations of **5** seems to exclude a competitive behavior for this compound (see Table S1 in the Supplementary data).

2.3. Leishmanicidal activity

The TryS inhibitors **1**–**6** were tested *in cellulo* to assess their potential as new leishmanicidal drug candidates. Their antileishmanial activity was monitored in axenic amastigotes of *L. infantum* by the resazurin assay. Cytotoxicity was evaluated in the human hepatoma cell line HepG2 by the crystal violet method. Half-maximal effective and cytotoxic concentrations (EC_{50} and CC_{50}, respectively) were compared to those of the reference drug miltefosine. According to the results shown in Table 2, only **1** (EC_{50} = 21.5 μM), **3** (EC_{50} = 7.3 μM) and **5** (EC_{50} = 0.4 μM) showed EC_{50} values below 25 μM. These three compounds were further tested for their leishmanicidal activity in amastigote-infected THP-1 cells. **1**, **3** and **5** were active against intracellular amastigotes but only **5** displayed submicromolar activity (0.6 μM) and, what is even

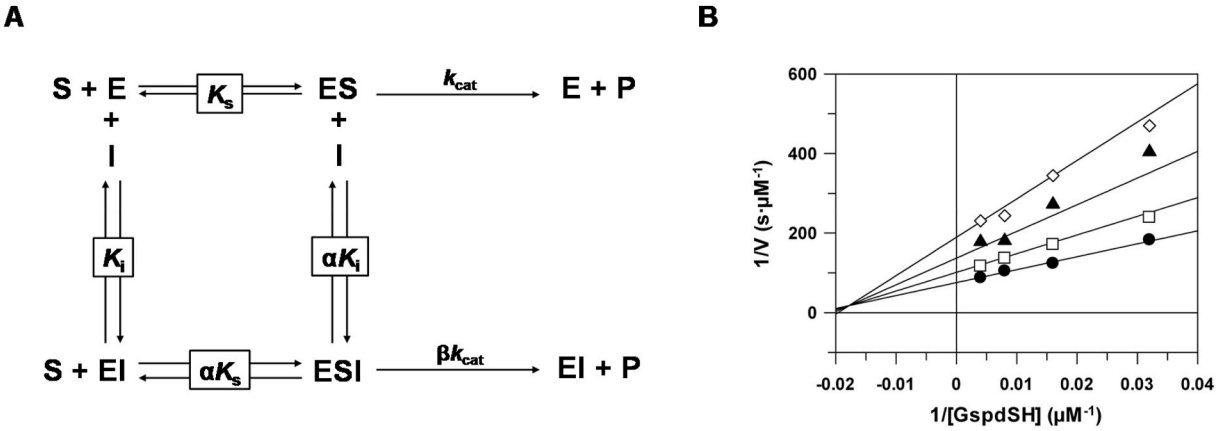

Fig. 5. Hyperbolic mixed inhibition of *Li*TryS by hit **4**. (**A**) Kinetic model of hyperbolic mixed inhibition. The inhibitor binds both to the free (E) and substrate-bound (ES) forms of the enzyme. The ESI complex is able to catalyze the ATP-dependent ligation of the polyamine substrate (either Spd or GspdSH) to a GSH molecule but at a much slower rate than the ES complex does. (**B**) Lineweaver-Burk double-reciprocal plot of the initial velocity of the *Li*TryS ligase reaction as a function of the GspdSH concentration measured at different concentrations of **4**: 0 μM (●), 0.5 μM (□), 1.6 μM (▲) and 5 μM (◇). Lines shown in the plot were obtained by fitting the reciprocal data to Equation (5). Results are representative of three independent experiments.

Table 2
Leishmanicidal activity, cytotoxicity and selectivity indices for selected compounds **1–6**.

Compound	EC_{50} Axenic Amastigotes (μM)[a]	EC_{50} Intracellular Amastigotes (μM)[b]	CC_{50} HepG2 (μM)[c]	SI[d]
Miltefosine	0.5 ± 0.005	0.7 ± 0.07	>75	>107
1	21.5 ± 2.4	13.5 ± 0.9	15.9 ± 0.4	1.2
2	47.6 ± 6.6	–	–	–
3	7.3 ± 0.5	17.9 ± 0.4	>75	>4.2
4	43.7 ± 4.3	–	–	–
5	0.4 ± 0.03	0.6 ± 0.1	21.3 ± 2.2	35.5
6	>75	–	–	–

[a] Half-maximal effective concentration (EC_{50}) ± standard error (SE) defined as that causing a 50% reduction of proliferation in *L. infantum* axenic amastigotes after a 24-h treatment. Results are representative of three independent experiments.

[b] EC_{50} is defined as that causing a 50% reduction in the number of *L. infantum* amastigotes per THP-1-derived macrophage in the culture after a 72-h treatment. Results are representative of three independent experiments.

[c] Half-maximal cytotoxic concentration (CC_{50}) is defined as that causing a 50% reduction of proliferation in human hepatocellular carcinoma (HepG2) cells after a 72-h treatment. Results are representative of three independent experiments.

[d] Selectivity index (SI) is the ratio of CC_{50} against HepG2 cells relative to EC_{50} against *L. infantum* intracellular amastigotes.

more important, a high selectivity index of 35.5. These two features make **5** a very promising candidate in the search for new leishmanicidal molecules. It must be pointed out that this high activity against *L. infantum* amastigotes is difficult to explain exclusively in terms of its inhibitory activity against TryS, so further biological characterization will be required to identify other possible molecular targets.

It is noteworthy that amphiphile **5** shows structural similarities to the alkyl-lysophospholipids (ALPs) group of compounds (See Fig. S1 in the Supplementary data) [27], a family with recognized anti-leishmanicidal activities among which miltefosine stands out as one of the most relevant drugs against leishmaniasis. Similarities between **5** and miltefosine seem to go beyond their structure, as both molecules induce similar changes in the $DiBAC_4(3)$-, TMRM-, and DHE-derived fluorescence of the parasites (see Fig. S3 in the Supplementary data). These alterations are indicative of depolarization of the plasma membrane, mitochondrial inner membrane and increase in the intracellular superoxide radical concentration, respectively. Surprisingly, miltefosine is also able to inhibit TryS (IC_{50} = 45.6 ± 4.7 μM; see Fig. S3D in the Supplementary data), even though its activity is weaker than that observed for **5**. These data reveal a new and unexpected mechanism of action for miltefosine.

Finally, it is also worth mentioning that **1** is part of a large family of TryR inhibitors discovered in our laboratory [23]. In fact, this hit could set the basis for the finding of molecules that can inhibit both TryR- and TryS-mediated $T(SH)_2$-(re)generating pathways.

2.4. Three-dimensional structure of LiTryS

We used molecular modeling, combined with molecular dynamics (MD) simulations, to provide mechanistic details of TryS, a monomeric ATP-dependent C—N ligase belonging to the ATP-grasp superfamily [28], and to shed light on the mode of substrate binding.

Even though the structural elucidation of TryS of *Leishmania major* (*Lm*TryS) in 2008 was an important milestone that helped in the understanding of the protein domain architecture and the organization of the distinct synthetase and amidase active sites [15], the amino acid stretch comprising residues 552 to 578, which includes the phosphate-binding loop (P-loop) that keeps the ATP molecule firmly in place, was not visible in the electron density map. Furthermore, this apo form of the enzyme did not directly inform about the positioning of substrates and co-substrates during catalysis. Fortunately, the crystal structure of *E. coli* GspdSH synthetase (*Ec*GspS) −which reveals a root-mean-square deviation (rmsd) of only 1.5 Å with the synthetase domain of *Lm*TryS, despite a low sequence identity (~30%), has been solved not only in the apo form but also in complex with (i) ADP and Mg^{2+} ions, (ii) the non-hydrolyzable ATP analogue AMPPNP and Mg^{2+} ions, (iii) GSH (whose cysteine thiol reacted to form a disulfide bond with Cys338 −not present in the equivalent position of *Lm*TryS and *Li*TryS− and whose Gly's carboxylic group formed an isopeptide bond with N^{ε} of Lys607), and (iv) a nanomolar phosphinate inhibitor that became phosphorylated during crystallization [29]. Hence, this bonded ligand is a phosphorous-containing pseudopeptide that resembles the tetrahedral intermediate formed upon nucleophilic addition of Spd to the acylphosphate of GSH and mimics GspdSH, although it contains two D-amino acids (D-Glu and D-Ala in place of L-Glu and L-Cys, respectively). This means that, although valuable and informative −particularly regarding the bound nucleotides at the S1 site (Fig. 6A), the Mg^{2+} ions and the P-loop−, the binding modes observed in the crystals do not necessarily match the productive binding poses for GSH in site 2 (the first GSH-binding site, as named in Ref. [15]) and for Spd or GspdSH in site 3 (the second GSH-binding site and the Spd-binding site, as named in Ref. [15]) prior to phosphorylation by ATP and subsequent nucleophilic attack. This is especially true for the GSH molecule that is covalently bonded to Cys338 at the S3 site and not suitably oriented for the reaction to take place. We speculate that this could be an artifact arising from (i) breakage of a putative disulfide bond between Cys338 and the spatially vicinal Cys596 caused by the 5 mM DTT used in crystallization, and (ii) mixed disulfide bond formation with GSH that imposes an alternative bound orientation. Besides, phosphoryl transfer from ATP to GSH only takes places upon binding of Spd (or GspdSH) because in the absence of the latter substrates only marginal ATPase activity of TryS was detected [30]. Therefore, to become further glutathionylated at the same reaction center that gave rise to GspdSH, this same metabolite has to change its position (and orientation) either by leaving the site completely −as does ADP− to rebind thereafter or by pivoting about the bound terminal amino group so that a new GSH molecule is allowed to occupy site 2 to become acylated by a new ATP molecule located in site 1 prior to the second nucleophilic addition that finally yields $T(SH)_2$. The latter mechanism would entail some sort of rotating/sliding motion of the Spd part of the newly formed GspdSH to reorientate and approach its free amino N^8 atom to the GSH carboxylate for the second glutathionylation event.

2.5. Catalytic mechanism of LiTryS

To try and solve the abovementioned problems, we model-built —in a stepwise manner— five different complexes of the synthetase domain of *Lm*TryS (Fig. 6A) so as to cover the main steps of $T(SH)_2$ biosynthesis. Each complex was subjected to MD simulations (≥150 ns each) for equilibration and conformational sampling in aqueous solution. By following this procedure, we were able to obtain a complete set of snapshots (Fig. S4 in the Supplementary data) describing in atomic detail (Fig. 6B—F) the most likely sequence of events leading from substrate binding to product release, as reported previously for other enzymes [31–33]. Significantly, the whole process appears to require just one reaction center, in good agreement with a previous independent proposal [34].

The initial Michaelis complex −consisting of the TryS domain with bound ATP$(Mg^{2+})_2$, GSH and Spd (Fig. 6B)− provided a consistent picture of the near-attack conformation (NAC) together with a rationale for the non-random substrate binding order, that is, for the finding that Spd binding at site 3 is strongly dependent on previous occupancy of sites 1 and 2 by ATP and GSH, respectively [30]. In fact, simulation of a similar complex lacking only Spd led to a stable but non-productive complex in which the γ-phosphate of ATP and the free carboxylate of GSH were found in locations incompatible with direct phosphoryl transfer (Fig. S4B in the Supplementary data). In both cases, the P-loop

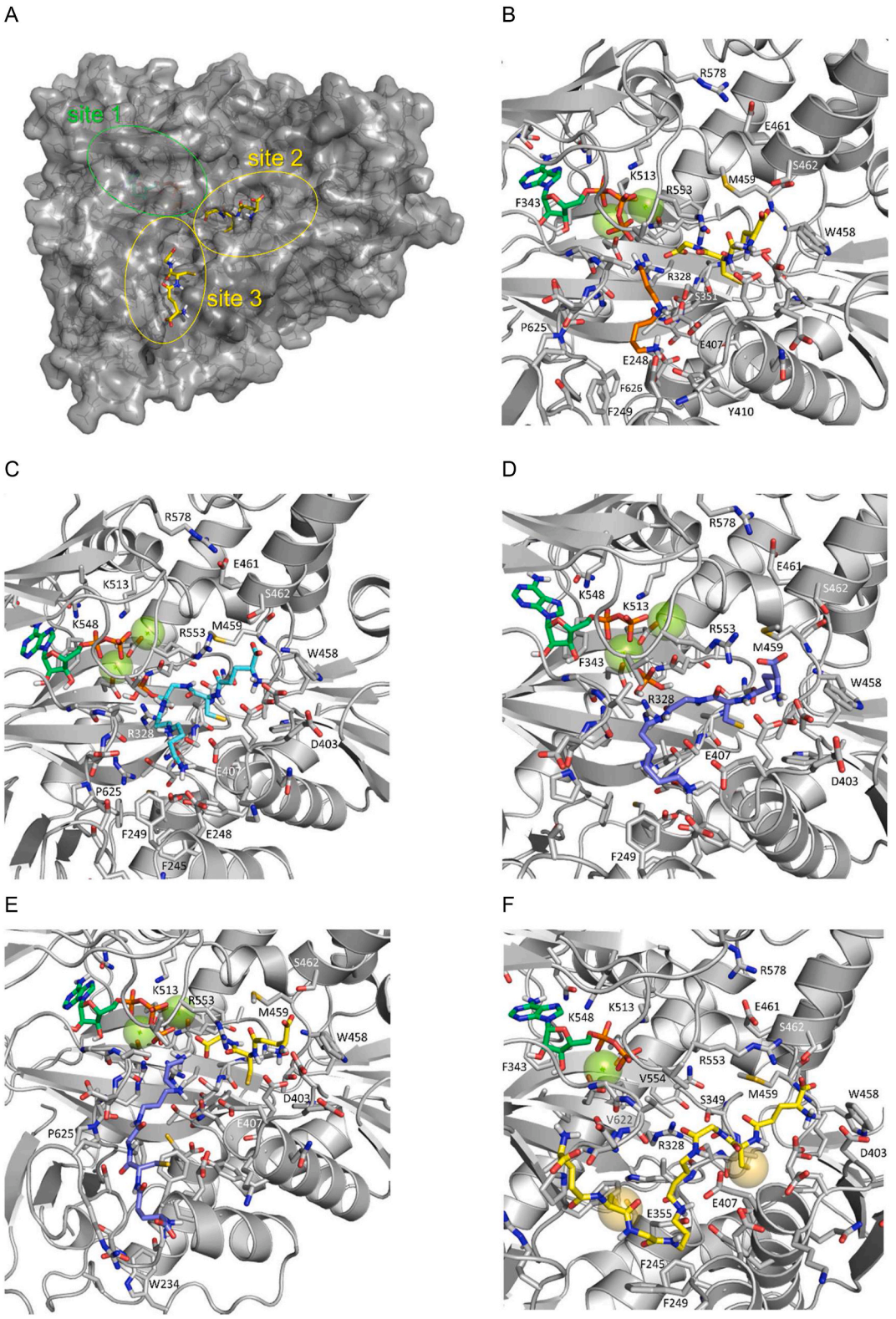

Fig. 6. Representative snapshots of *Li*TryS throughout the simulated catalytic cycle. (**A**) 3D model of the C-terminal ligase domain of *Li*TryS enveloped by a semitransparent surface. Site 1 where ATP (green sticks) binds, and sites 2 and 3 for GSH (yellow sticks) binding in the first and second nucleophilic additions, respectively, are circled. This naming convention follows that reported in Ref. [15]. (**B**) TryS:ATP$(Mg^{2+})_2$:GSH:Spd, first Michaelis complex. (**C**) TryS:ADP$(Mg^{2+})_2$:[APG:Spd]*, transition state. (**D**) TryS:ADP$(Mg^{2+})_2$:N^1-GspdSH plus leaving $H_2PO_4^-$. (**E**) TryS:ATP$(Mg^{2+})_2$:GSH:N^1-GspdSH, second Michaelis complex. (**F**) TryS:ADP(Mg^{2+}):$T(SH)_2$, enzyme-product complex, with the thiol groups as spheres. C atoms have been colored lime green in ATP, yellow in GSH and $T(SH)_2$, violet in GspdSH, cyan in the transition state, and orange is free Spd. Mg^{2+} ions are displayed as spheres. The side chains of relevant residues discussed in the text have been labeled and are shown as sticks. Water molecules and neutralizing K^+ counterions have been omitted to enhance clarity.

(^{551}VGRVGS^{556}) is found in a closed conformation, with the essential Arg553 [35] in an extended conformation and Val554 establishing a hydrophobic seal with Val622 that partly shields the nucleotide from the solvent.

Two ATP γ-phosphate oxygens are fixed in position by Arg613 and another one forms an ion pair with the essential Arg328 [29], which in turn is hydrogen-bonded to Asp330. Tight binding and proper orientation of Spd rely on electrostatic attraction between the side-chain carboxylates of Glu355 and Glu407 and the central secondary amino group (N^5) −with the assistance of Ser351 and Tyr410−, and repulsion by the guanidinium of Arg613; the terminal N^8, in turn, hydrogen-bonds to the carboxylates of Asp252 and Asp623, whereas the attacking N^1 is close to one of the ATP γ-phosphate oxygens that presumably abstracts one proton to trigger the nucleophilic attack. GSH is flanked by the indole ring of Trp458 on the zwitterion side −whose carboxylic moiety is held in place through hydrogen bonds with the backbone NH of Met459 and the side-chain hydroxyl of Ser462 whereas the ammonium group is grasped by the carboxylates of Asp403 and Glu408− and the guanini-dium group of Arg328 on the Gly carboxylate side, with the Cys thiol buried between the side-chain hydroxyls of Ser349 and Ser351. In fact, we propose that residues ^{349}SAS^{351} act as a molecular toggle switch that responds to binding of GSH and Spd. These substrates impose a definite backbone orientation of this amino acid stretch that acts in concert with the rotameric state of Arg328 to allow GSH and Spd to achieve the NAC as a prerequisite for enzymatic function.

Once the γ-phosphate of ATP has been transferred to the glycine carboxylate of GSH −and occupies a position similar to that observed in N^5-carboxyaminoimidazole ribonucleotide synthetase upon ATP hydrolysis [36]−, the deprotonated amino N^1 of Spd can effect the nucleophilic attack at the acylphosphate's carbonyl to give rise to the unstable tetrahedral intermediate (Fig. 6C) that finally collapses to produce N^1-GspdSH and a free phosphate as H_2PO4^- (Fig. 6D). It is noteworthy that the Spd part of the transition state of the reaction showed much higher mobility than Spd itself in the Michaelis complex (*cf.* **C** and **B** in Fig. 6), a finding that is likely to be related to facilitation of product release. Indeed, the fully solvated Mg^{2+} and H_2PO4^- ions, the Mg^{2+}-bound ADP, and N^1-GspdSH must leave their respective binding pockets to make room (i) in site 1 for ATP −for which Phe343 provides a docking platform to the adenine and Lys513 and Lys548 most of the electrostatic driving force to attract the phosphates−, and (ii) in site 2 for a second GSH molecule. In this scenario, N^1-GspdSH binds with the Spd portion in a similar arrangement to that described above for Spd −but with N^8 now approaching the acylphosphate− and the GSH part docked in a site not present in *Ec*GspS that is largely made up by an insertion corresponding to the Gly250–Val262 stretch (Fig. 6E). We speculate with the possibility that the rebinding event for N^1-GspdSH might involve a flipping motion of a partially bound molecule for this orientation reversal, given the presence in this region of many aromatic residues −some of them seen to alternate between different rotameric states along the reaction coordinate, *e.g.* Phe249 and Phe626− that would allow the formation of cation-π interactions, as seen in the complex of Spd with *E. coli* PotD protein [37]. Finally, the second glutathionylation event ligates N^8 of N^1-GspdSH to GSH to yield a molecule of the final product, $T(SH)_2$ (Fig. 6F).

Throughout the catalytic cycle, we found that four arginine residues play crucial roles and change their rotameric state to perform different functions. In sequential order, the first one is Arg328, which acts in concert with residues ^{349}SAS^{351} to operate the putative molecular toggle switch that responds to binding of GSH and Spd, as explained above; the second one is Arg538, which also presents different rotamers in the *Ec*GspS crystal structures depending on the nature of the bound ligand [29]; the third one is Arg553, which can adopt both an extended conformation that allows hydrogen bond formation with the zwitterion carboxylate of GSH and a more folded rotameric state in order to fixate the Cys carbonyl of GSH during the nucleophilic attack by either Spd or GspdSH; and the fourth one is Arg613, which changes its conformation completely so as to interact with either the γ-phosphate of ATP or the loop encompassing Val622.

Taken together, our simulation results provide evidence that the large Y-shaped cavity where catalysis takes place in the ligase domain of *Li*TryS is subtly malleable in response to the different natural substrates (and combinations thereof) and provides ample room for inhibitor binding. Furthermore, the atomic models account for the facts that (i) both GSH and $T(SH)_2$ —at high concentrations— act as inhibitors of this enzymatic activity [38], and (ii) GSH can be ligated to either Spd or GspdSH [39]. In view of our simulation results, TryS inhibition by GSH most likely occurs because of binding to part of site 3 –where the GSH portion of GspdSH binds in the reaction leading to $T(SH)_2$ (Fig. 6A).

2.6. Binding modes of LiTryS inhibitors **1** and **3**

Representative *Li*TryS structures obtained throughout the simulated catalytic cycle were used as target receptors for the automated ligand docking procedure to gain insight into plausible binding modes for *LiTryS* inhibitors **1** and **3**. In Fig. 7 we show the top-scoring poses that are compatible with the biochemically characterized mechanism of inhibition. In brief, **3** would bind in the vicinity of site 3, thereby competing with Spd and GspdSH; in contrast, **1** appears to locate its free amino group in the same place that recognizes the amino group of adenine of ATP bound in site 1 whereas its imidazolidinone would project into the Spd-binding pocket in site 3. As a control of docking performance, we used (i) DDD60632, which is known to display characteristic mixed inhibition with respect to Spd, and (ii) DDD66604, a standard TryS inhibitor that is competitive with respect to Spd [12]. Both inhibitors found ready accommodation in the Spd-binding site (Fig. 7C−D).

3. Conclusions

Two different methodologies have been used to search for *Li*TryS inhibitors using a chemically diverse in-house library of molecules (n = 144). Six of them, grouped in three distinct structural classes, displayed IC_{50} values below 15 μM. Among them, compounds **1** and **3** display a classical competitive mechanism of inhibition against the polyamine substrates with K_i values in the low micromolar range whereas **4** shows a mixed hyperbolic inhibition against the same substrate and a K_i value in the nanomolar range. Because of its noncompetitive behaviour, the strong inhibitory activity of **4** is not expected to be impaired by increased concentrations of Spd. Additionally, a competitive inhibition against ATP could be observed for **1**. Molecular modeling combined with MD simulations shed light on the mode of substrate binding and provided mechanistic details of the ligase reaction catalyzed by *Li*TryS. Representative protein structures from the simulated trajectories were used for automated ligand docking. The top-scoring poses locate **1** in a position that simultaneously overlaps the binding sites of ATP and Spd/GspdSH whereas **3** would bind in the vicinity of site 3, thereby competing exclusively with Spd/GspdSH. To our knowledge, this is the first report of a molecule whose binding site overlaps sites 1 and 3, which explains the competitive mode inhibition of **1** against both substrates. It is worth mentioning that **1** is part of a large family of TryR inhibitors discovered in our laboratory [23] so this hit could set the basis for the finding of molecules that can inhibit both TryR- and TryS-mediated $T(SH)_2$-(re)generating pathways. Compounds **1**, **3** and **5** were active against intracellular amastigotes. The excellent EC_{50} of 0.6 μM and an SI value of 35.5 obtained for **5** together with its capacity to induce depolarization of the mitochondrial inner membrane make this hit a very promising candidate in the search for new leishmanicidal molecules. These hit molecules represent the first steps to the race to have preclinical candidate molecules that will require a hit-to-lead optimization of their drug-like properties, through an extensive medicinal chemistry program, to become good preclinical leishmanicidal inhibitors.

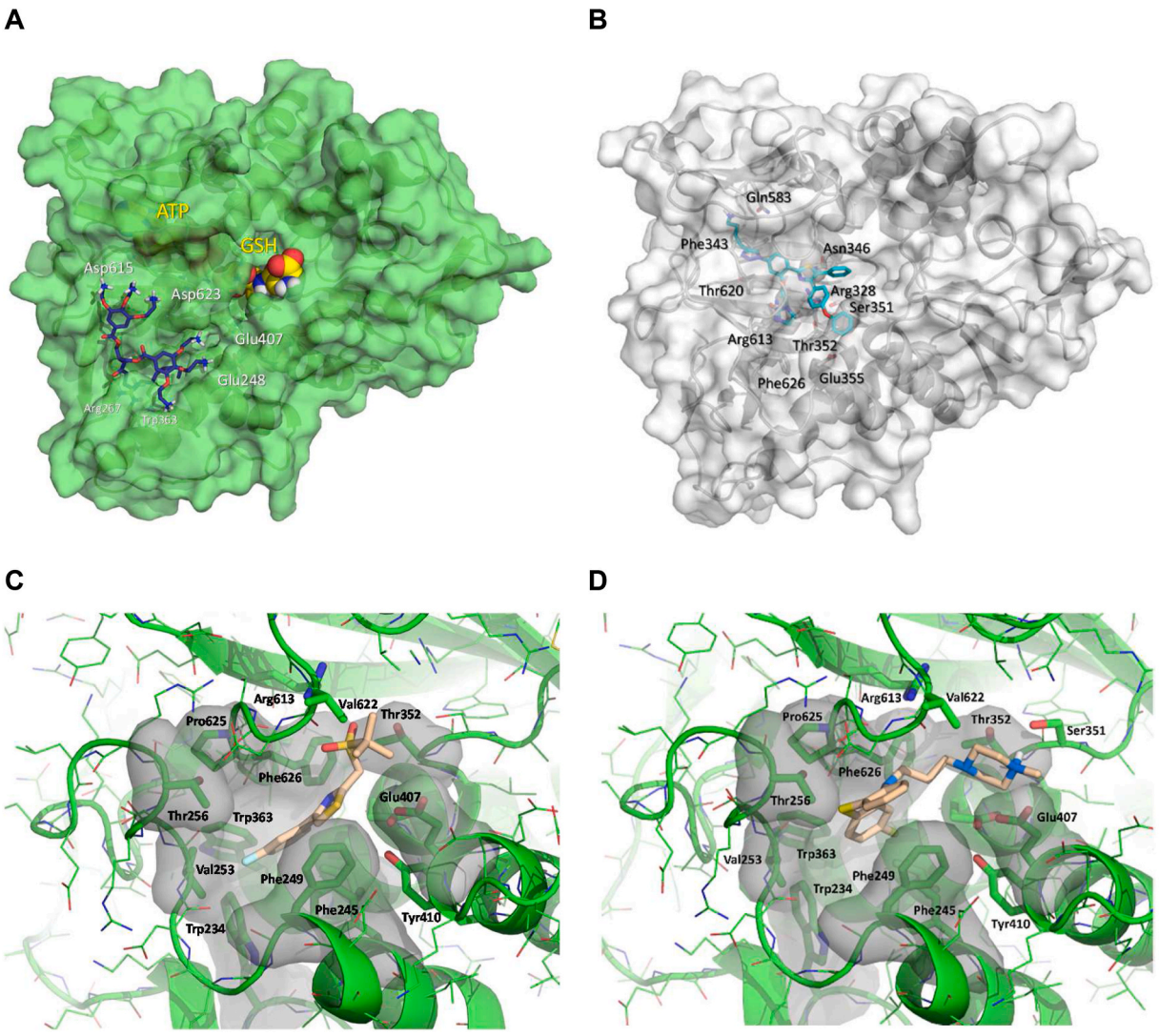

Fig. 7. Docking results showing the most likely binding poses for (**A**) **3** (sticks, C atoms in violet), (**B**) **1** (sticks, C atoms in cyan), (**C**) DDD60632 [12] (sticks, C atoms in cream), and (D) DDD66604 [12] (sticks, C atoms in cream). In (**A**) and (**B**) a semitransparent surface has been displayed to highlight the binding pockets. In (**A**) ATP and GSH are shown for reference as CPK models with C atoms colored in yellow.

4. Experimental

4.1. Chemistry

4.1.1. Compound synthesis

The syntheses of the compounds used in this study have been described in references 23–26. The full characterization, purity data and previous biological activities of these compounds have been also included in the Supplementary material. The detailed synthetic process, characterization, and purity of the new compound **5** are reported in the Supplementary data.

4.2. Biological methods

4.2.1. Compound library handling

The compound library was supplied by the Medicinal Chemistry Institute of the Spanish Research Council in two different 96-well microplates (10 μL/well), each containing 72 chemical entities. Stock solutions of these compounds were prepared in anhydrous DMSO (Sigma-Aldrich, Saint Louis, MO) at 10 mM. The thirteen hits were later supplied in powder form and stock solutions were prepared in anhydrous DMSO (Sigma-Aldrich, Saint Louis, MO) at 15 mM. Aliquots were stored at −20 °C.

4.2.2. Materials and reagents

All reagents for the *in vitro* enzymatic and *in cellulo* activity assays were obtained from Sigma-Aldrich (Saint Louis, MO) except for N^1-glutathionylspermidine disulfide, BIOMOL® Green reagent, RPMI-1640 with L-glutamine and M199 mediums, which were purchased from Bachem (Bubendorf, Switzerland), Enzo Life Sciences (Farmingdale, NY), Lonza (Basel, Switzerland) and Gibco (Leiden, The Netherlands), respectively.

4.2.3. Cloning, expression and purification of LiTryS

The DNA coding sequence for *Li*TryS (TriTryp DB: LinJ.27.1770; NCBI Reference Sequence: XM_001466389.1; UniProt: A4I2Z3) was polymerase chain reaction (PCR)-amplified using genomic DNA extracted from *L. infantum* promastigotes (MCAN/ES/89/IPZ229/1/89) as template and the following primers: *Li*TryS-Fw (5′GGGGGATCC*CTGGAAGTTCTGTTCCAGGGGCCC***ATG**TCGTCTCTGCCGCG3′), containing a *BamHI* site (underlined) separated from the start codon (bold) by the DNA sequence of the PreScission protease recognition site (on italic) which was introduced to remove the N-terminal tags, and *Li*TryS-Rv (5′CCCCTCGAG**TTA**CTCGTCCTCGGCCATC3′),

containing an *XhoI* site (underlined) and a stop codon (bold). The PCR product was double digested with *BamHI* and *XhoI*, and subsequently cloned into pET-28a(+) vector (Novagen, Madison, WI) downstream the N-terminal polyhistidine (HIS)-tag region to generate the *pET28a-HIS-LiTryS* construct. Following transformation into *Escherichia coli* strain DH5α, plasmid DNA was extracted from overnight bacterial cultures of independent clones, and double digested with *BamHI* and *XhoI*. Digestion products were run on a 1% agarose gel and the sizes of the vector backbone, and the insert was analyzed. The identity of the *Li*TryS sequence of *pET28a-HIS-LiTryS* constructs extracted from two independent clones showing the expected digestion pattern was verified by DNA sequencing.

His-tagged recombinant *Leishmania infantum* TryS (*Li*TryR) was purified from BL21 (DE3) Rossetta *E. coli* transformed with *pET28a-HIS-LiTryS* construct. An overnight *E. coli* culture (50 mL) grown at 37 °C in LB medium with suitable antibiotics and vigorous shaking was used to inoculate (1:100) fresh LB medium supplemented with the same antibiotics. The scaled-up *E. coli* culture was allowed to grow in the same conditions until a OD_{600} of 0.5 was reached. *Li*TryS expression was induced upon addition of 0.5 mM isopropyl-β-D-1-thiogalactopyranoside (Thermo Scientific, Waltham, MA) during 16 h at 26 °C. Cells were harvested by centrifugation at 9,000*g* and 4 °C and the wet pellets were resuspended in buffer A (50 mM Tris pH 8, 200 mM NaCl, 5 mM $MgCl_2$ and 25 mM imidazole) containing 1 mg/mL lysozyme and a protease inhibitor cocktail. Following a 30 min incubation on ice, the cell lysate was disrupted by sonication on ice (50% pulses, potency 7) for 30 min using a Sonifier Cell Disruptor B15 (Branson, Danbury, CT, USA) and centrifuged during 1 h at 50,000*g* and 4 °C. Supernatant was collected and sonicated again as previously described for additional 10 min. The clarified supernatant containing the soluble protein fraction was filtered using a sterile syringe filter with a 0.45 μm pore size hydrophilic PVDF membrane and subsequently loaded onto a HisTrap column (GE Healthcare, Chicago, IL, USA) for 16 h at 4 °C using a peristaltic pump P-1 (GE Healthcare, Chicago, IL, USA). The HisTrap column was then connected to an ÄKTA purifier UPC 10 (GE Healthcare, Chicago, IL, USA) and extensively washed using 25 mL of a 10% fixed gradient between buffers A and B (50 mM Tris pH 8, 200 mM NaCl, 5 mM $MgCl_2$ and 500 mM imidazole). *Li*TryS was isocratically eluted using a 40% fixed gradient between buffers A and B. Fractions containing recombinant *Li*TryS were pooled and loaded onto a HiPrep™ 26/10 Desalting column (GE Healthcare, Chicago, IL, USA) previously equilibrated with buffer A to remove imidazole. Protein concentration was determined using the theoretical values for the molar extinction coefficient and molecular weight of the different *Li*TryS versions using a NanoDrop™ spectrophotometer (Thermo Scientific, Waltham, MA). Finally, *Li*TryS was concentrated to 2 mg/mL using an Amicon® Ultra-15 30K (Merck Millipore, Burlington, MA, USA) and an equal volume of glycerol was added before storing at −20 °C.

4.2.4. LiTryR purification

HIS-tagged recombinant *Leishmania infantum* TryR (*Li*TryR) was purified from *E. coli*, as already explained for the HIS-tagged version of recombinant *Li*TryS. but inducing protein expression upon addition of 1 mM isopropyl-β-D-1-thiogalactopyranoside (Thermo Scientific, Waltham, MA) instead of 0.5 mM during 16 h at 26 °C.

4.2.5. Standard LiTryS ligase activity assay

ATP-dependent ligase reactions catalyzed by *Li*TryS were performed in 96-well microplates (50 μL/well) at 37 °C in 100 mM HEPES buffer pH 8 containing 0.5 mM EDTA, 10 mM $MgCl_2$, 150 μM ATP, 100 μM GSH, 100 μM DTT, 2 mM Spd, 2% DMSO, 0.1% glycerol and 25 nM recombinant *Li*TryS. For the enzymatic reactions performed with GspdSH (500 μM) instead of Spd, a stock solution of N^1-glutathionylspermidine disulfide (2.5 mM) was prepared in HEPES (100 mM HEPES pH 8) containing DTT (2.75 mM) to achieve complete reduction of N^1-glutathionylspermidine disulfide to GspdSH. DTT, DMSO and glycerol concentrations used in this assay do not have any relevant effect on the kinetics of the *Li*TryS ligase enzymatic reactions. For the primary screening, test compounds prepared at 1.25 mM in anhydrous DMSO were transferred (1 μL/well) to the 96-well assay plates and a master mix containing all of the reaction components except *Li*TryS (1.72-fold their end concentration in the assay) was added (29 μL/well). For all IC_{50} determinations, test compounds were serially diluted to generate 6-point inhibitor dose-response curves. For IC_{50} determinations at conditions in which one specific substrate concentration is reduced to its K_m value, ATP, GSH, Spd and GspdSH concentrations were individually adjusted to 35 μM, 45 μM, 450 μM and 30 μM, respectively. Reactions were started by adding 20 μL of a solution containing 100 mM HEPES pH 8 and 62.5 nM *Li*TryS. Blank controls were prepared by adding 20 μL of 100 mM HEPES buffer pH 8 instead of *Li*TryS. Reactions were run at 37 °C for 30 min and stopped with BIOMOL Green reagent (200 μL/well). BIOMOL Green signal due to phosphate release during *Li*TryS ligase reaction was allowed to develop for 30 min before the absorbance of each well was read at 650 nm (A_{650nm}) using an EnSpire Multimode Plate Reader (PerkinElmer, Waltham, MA).

The percentage of *Li*TryS enzymatic activity was calculated as follows. The A_{650nm} of the blank controls was subtracted to the A_{650nm} of the reactions in the presence of DMSO or test compounds to obtain the A_{650nm} increment (ΔA_{650nm}) of the vehicle and each of the test compounds, respectively. The ΔA_{650nm} in the presence of the test compounds were then normalized as a percentage with respect to the ΔA_{650nm} in the presence of DMSO.

For IC_{50} determinations, the percentages of *Li*TryS activity in the presence of different concentrations of a test compound were fitted to a nonlinear regression model with the GraFit 6 software (Erithacus, Horley, Surrey, UK). All the assays were conducted in triplicate in three independent experiments.

4.2.6. DTNB/LiTryR-coupled LiTryS ligase activity assay

ATP-dependent ligase reactions catalyzed by *Li*TryS were performed as explained above. After 30 min, *Li*TryS ligase reactions were stopped by adding 50 μL of a 100 mM HEPES pH 8 containing 500 μM DTNB which oxidizes all the low molecular weight thiols [GSH, GspdSH and $T(SH)_2$]. A master mix containing 100 mM HEPES pH 8, 7.9 mM EDTA, 78.9 μM $NADP^+$ and 394.7 μM NADPH was added (95 μL/well). *Li*TryR oxidoreductase reactions were started by adding 55 μL of a solution containing 100 mM HEPES pH 8 and 45.4 nM *Li*TryR. The final 250 μL DTNB/*Li*TryR-coupled *Li*TryS ligase activity assay contained 100 mM HEPES pH 8, 3.1 mM EDTA, 30 μM $NADP^+$, 100 μM DTNB, 150 μM NADPH, 20 μM DTT, 2 mM $MgCl_2$, 0.08% glycerol, 0.65% DMSO, and 10 nM recombinant *Li*TryR. *Li*TryR oxidoreductase activity was monitored for 1 h at 26 °C by measuring the absorbance at 412 nm due to TNB generation in an EnSpire Multimode Plate Reader (PerkinElmer, Waltham, MA).

The initial rates of the reactions were estimated from the slope at the origin of the reaction progress curves. The initial velocities in the presence of different inhibitors were normalized as a percentage with respect to the initial velocity in the presence of the inhibitor vehicle (DMSO).

4.2.7. Determination of compound inhibitory constants

To establish the modality of inhibition of the lead compounds, data sets were collected at four inhibitor concentrations with four varied concentrations of the putative substrate competing with each of the lead compounds for binding to *Li*TryS. The inhibitory constants were calculated following a slightly modified version of the standard *Li*TryS ligase activity assay explained above. Inhibitors were serially diluted in DMSO and manually dispensed into the appropriate wells of a 96-well microplate (1 μL/well). The variable substrate (ATP or GspdSH) was serially diluted in 100 mM HEPES buffer pH 8 and the solutions containing different substrate concentrations were mixed with a master mix containing the rest of the reaction components except *Li*TryS. The resulting

mixtures were then added to the 96-well microplate (29 μL/well). When ATP was the variable substrate, the final concentrations tested in the 50 μL *Li*TryS ligase assay ranged from 400 to 50 μM, while Spd and GSH were fixed to 2 mM and 100 μM, respectively. When GspdSH was the variable substrate, the final concentrations were varied from 250 to 31.2 μM, while ATP and GSH were fixed to 150 μM and 100 μM, respectively. Reactions were started by adding a solution containing 100 mM HEPES pH 8 and 62.5 nM *Li*TryS (20 μL/well). The order of addition of the different solutions was critical to avoid enzyme pre-incubation with the inhibitor or the substrates. Reactions were run at 37 °C for 30 min and stopped with BIOMOL Green reagent (200 μL/well). BIOMOL Green signal was allowed to develop for 30 min before the absorbance of each well was read at 650 nm using an EnSpire Multimode Plate Reader (PerkinElmer, Waltham, MA).

4.2.8. Leishmania cell lines and culture

L. infantum promastigotes (MCAN/ES/89/IPZ229/1/89) were grown in RPMI-1640 with L-glutamine medium supplemented with 10% heat-inactivated fetal calf serum (FCS), 100 units/mL penicillin and 100 μg/mL streptomycin (Gibco, Leiden, The Netherlands), and 25 mM HEPES pH 7.2 at 26 °C. *L. infantum* axenic amastigotes (MCAN/ES/89/IPZ229/1/89) were grown in M199 medium supplemented with 10% heat-inactivated FCS, 0.4 mg/L hemin, 100 units/mL penicillin and 100 μg/mL streptomycin (Gibco, Leiden, The Netherlands), 10 mg/L gentamicine, 100 mg/L L-asparagine, 50 mg/L sodium pyruvate, 200 mg/L sucrose, 1 g/L β-alanine, 320 mg/L malic acid, 40 mg/L fumaric acid, 70 mg/L succinic acid, 200 mg/L α-ketoglutaric acid, 300 mg/L citric acid, 1.1 g/L sodium bicarbonate, and 5 g/L MES pH 5.4 at 37 °C.

4.2.9. Axenization of L. infantum promastigotes

Axenization was performed by inoculating 0.5 mL of a 7-day stationary phase culture of *L. infantum* promastigotes (approximately ~2-3x10^7 parasites/mL) in 4.5 mL of amastigotes medium and incubating the culture at 37 °C for 5–7 days. Axenization of L. *infantum* promastigotes was followed by phase-contrast microscopy in an Eclipse Ti inverted microscope (Nikon, Tokyo, Japan).

4.2.10. Leishmanicidal activity

L. infantum axenic amastigotes from logarithmic cultures were seeded at a concentration of 10^6 parasites/mL (200 μL/well) in 96-well Nunclon™ Delta Surface microplates (Nunc, Roskilde, Denmark). Drug treatments were subsequently performed for 24 h at 37 °C. This time period was selected to minimize the probability of selecting cytostatic molecules that would be poorly effective in the intracellular infection assay [40]. Microplates were sealed with parafilm during all the incubation periods. Parasite viability was evaluated using the resazurin/alamar blue fluorometric assay. Briefly, 5 μL of alamarBlue™ HS Cell Viability Reagent (Invitrogen, Leiden, The Netherlands) was added to the 96-well microplates. After a 24 h incubation at 37 °C and 5% CO_2, the color of the cell culture medium gradually changed from blue to pink due to intracellular enzymatic reduction of resazurin into resorufin, which is subsequently excreted into the medium. The cell culture media were transferred (100 μL/well) to black opaque 96-well microplates (PerkinElmer, Waltham, MA). Fluorescence due to resorufin production was measured at an emission wavelength of 590 nm using an excitation wavelength of 560 nm in an EnSpire Multimode Plate Reader (PerkinElmer, Waltham, MA).

For EC_{50} determinations, the percentage of live parasites was estimated by normalizing the resorufin fluorescence values obtained at each treatment condition to the value of the vehicle-treated controls. EC_{50} values for each compound were obtained by fitting these percentages to a nonlinear regression model with the GraFit 6 software (Erithacus, Horley, Surrey, UK). All the assays were performed in triplicate in three independent experiments.

4.2.11. Human cell lines culture

THP-1 cells were grown in RPMI-1640 medium with L-glutamine supplemented with 10% heat inactivated FCS, 100 units/mL penicillin and 100 μg/mL streptomycin (Gibco, Leiden, The Netherlands), 1 mM sodium pyruvate, and 10 mM HEPES pH 7.5 at 37 °C and 5% CO_2.

Liver hepatocellular carcinoma HepG2 cells were grown in DMEM medium supplemented with 10% heat inactivated FCS, 100 units/mL penicillin and 100 μg/mL streptomycin (Gibco, Leiden, The Netherlands), and 10 mM HEPES pH 7.5 at 37 °C and 5% CO_2.

4.2.12. In vitro infection of THP-1 derived macrophages with GFP-expressing L. infantum axenic amastigotes

THP-1 monocytes were seeded in 48-well Nunclon™ Delta Surface microplates (Nunc, Roskilde, Denmark) at a concentration of 5 x 10^5 cells/mL in RPMI complete medium supplemented with 100 ng/mL phorbol 12-myristate 13-acetate (PMA) (250 μL/well). PMA-differentiation of THP-1 monocytes to macrophages was allowed for 24 h at 37 °C and 5% CO_2. THP-1 derived macrophages were infected with GFP-expressing *L. infantum* axenic amastigotes at 5 x 10^6 parasites/mL in RPMI-1640 complete medium for 24 h (250 μL/well). Non-internalized amastigotes were washed out twice with PBS (250 μL/well). The remaining non-internalized parasites were challenged for 24 h with THP-1 medium supplemented with 10% horse serum (Gibco, Leiden, The Netherlands) instead of FCS (250 μL/well). Extracellular dead parasites were removed by aspiration and infected macrophages were washed twice with PBS (250 μL/well). Drug treatment of infected macrophages was performed in 500 μL of fresh RPMI-1640 medium supplemented with 10% horse serum. Following a 72-h incubation at 37 °C and 5% CO_2, treatments were removed by two PBS washes (500 μL/well).

Cytotoxicity of THP-1 infected macrophages was determined using the resazurin/alamar blue fluorometric assay. Briefly, alamarBlue™ HS Cell Viability Reagent (Invitrogen, Leiden, The Netherlands) was prepared in RPMI-1640 complete medium according to the manufacturer's instructions and subsequently added to the 48-well microplates (150 μL/well). After a 2-h incubation at 37 °C and 5% CO_2, the cell culture media were transferred (100 μL/well) to black opaque 96-well microplates (PerkinElmer, Waltham, MA). Fluorescence due to resorufin production was measured at an emission wavelength of 590 nm using an excitation wavelength of 560 nm in an EnSpire Multimode Plate Reader (PerkinElmer, Waltham, MA).

The excess of resazurin was aspirated from the 48-well microplates and the infected macrophages were washed once with PBS (500 μL/well). Lysis of infected macrophages was performed with 120 μL of SDS 0.005% (w/v) in PBS. After a 30 min incubation at 37 °C and 5% CO_2, the lysis was stopped upon addition of RPMI complete medium with 20 μg/mL propidium iodide (120 μL/well). The cell lysates were transferred to a 96-well microplate (200 μL/well) and the GFP + amastigotes extracted from the infected macrophages were acquired by a MACSQuant® Analyzer 10 flow cytometer (Miltenyi Biotec, Bergisch Gladbach, Germany) equipped with 405-nm (21.5 mW), 488-nm (30 mW) and 640-nm (40 mW) lasers. The number of GFP + amastigotes was obtained by using the MACSQuant® Analyzer's capacity of absolute cell counting. 20 μL of each sample were acquired using a medium flow rate automatically adjusted to maintain 1000 events/s.

Gate segmentation was performed as follows. First, the population of intracellular amastigotes (P1) was selected based on their forward scatter (FSC) and side scatter (SSC) values. The photomultiplier tube (PMT) voltages of channels FSC and SSC were adjusted to 445 V and 654 V, respectively, to distinguish the population of intracellular amastigotes and THP-1 cell debris. Live intracellular amastigotes belonging to P1 were identified due to their exclusion of propidium iodide (P1/P2), and their GFP-associated green fluorescence (P1/P2/P3). Propidium iodide was excited with the 488-nm laser and the fluorescence was collected through a longpass filter of 750 nm in the B4 fluorescence channel. GFP was excited with the 488-nm laser and the fluorescence

was collected through a bandpass filter of 525/50 nm in the B1 fluorescence channel. The PMT voltages of channels B4 and B1 were adjusted to 470 V and 535 V, respectively, to identify the population of live intracellular GFP + amastigotes.

For half-maximal cytotoxic concentration (CC_{50}) determinations, the percentage of live and infected macrophages was estimated by normalizing the resorufin fluorescence values obtained at each treatment condition to the value of the vehicle-treated controls. CC_{50} values for each compound were obtained by fitting these percentages to a nonlinear regression model with the GraFit 6 software (Erithacus, Horley, Surrey, UK).

For determining the EC_{50} values in *L. infantum* intracellular amastigotes, the relative number of GFP^+ intracellular amastigotes per macrophage in each sample was estimated by dividing the total number of GFP^+ amastigotes by the corresponding resorufin fluorescence value. Results were then normalized to the vehicle-treated controls. EC_{50} values for each compound were obtained by fitting these normalized results to a nonlinear regression model with the GraFit 6 software (Erithacus, Horley, Surrey, UK). All the assays were conducted in three independent experiments.

4.2.13. Determination of cellular toxicity

Liver hepatocellular carcinoma HepG2 cells were seeded in 24-well Nunclon™ Delta Surface microplates (Nunc, Roskilde, Denmark) at a concentration of 10^5 cells/mL at 37 °C and 5% CO_2 in DMEM complete medium and allowed to attach to the cell culture-treated surface of the microplates for 24 h. Drug treatment of HepG2 cells was performed during the logarithmic growth phase at 37 °C and 5% CO_2 for 72 h in DMEM medium supplemented with 10% horse serum to compare the cytotoxic effect of the compounds against HepG2 cells and *L. infantum* intracellular amastigotes. As performed in the infection experiments detailed above, DMEM medium was supplemented with 10% horse serum instead of 10% heat-inactivated FCS to compensate for any difference in terms of compound retention.

The cytotoxic activity of the compounds was evaluated by the crystal violet assay. Briefly, cells were washed with PBS and stained with crystal violet solution (0.2% crystal violet, 2% ethanol) for 10 min at room temperature (200 μL/well). The microplates were subsequently washed twice with tap water and allowed to dry. Finally, the stained cells were solubilized with 1% SDS (400 μL/well), and color intensity was quantified at 570 nm (A_{570nm}) using an EnSpire Multimode Plate Reader (PerkinElmer, Waltham, MA).

For CC_{50} determinations, the A_{570nm} of the blank controls (wells added with the medium alone) was substracted to the A_{570nm} of the cells treated with DMSO or test compounds to obtain the A_{570nm} increment (ΔA_{570nm}) of the vehicle and each of the test compounds, respectively. The ΔA_{570nm} in the presence of the test compounds were then normalized as a percentage with respect to the ΔA_{570nm} in the presence of DMSO. CC_{50} values for each compound were obtained by fitting these percentages to a nonlinear regression model with the GraFit 6 software (Erithacus, Horley, Surrey, UK). All the assays were conducted in three independent experiments.

4.2.14. Data and statistical analysis

The quality of the biochemical assays used in the primary screening was assessed by determining the Z' factor and the signal-to-background parmeters (S:B) using the following equations [41]:

$$Z' = 1 - \frac{(3\sigma_{max} + 3\sigma_{min})}{|\mu_{max} - \mu_{min}|} \quad (1)$$

$$S{:}B = \frac{\mu_{max}}{\mu_{min}} \quad (2)$$

where σ_{max} and σ_{min} are the standard deviations of the positive and negative controls, respectively, and μ_{max} and μ_{min} are the mean of the positive and negative controls, respectively.

All linear and nonlinear regressions used for kinetic data analysis were performed using GraFit 6.0 software (Erithacus, Horley, SRY, UK). All experiments were repeated at least three times to ensure the reliability of single values.

IC_{50}, EC_{50} and CC_{50} values were determined using the two-parameter IC_{50} equation provided by GraFit, where the lower data limit is 0%, and the upper limit is 100%:

$$y = \frac{100}{1 + \left(\frac{x}{IC_{50}}\right)^s} \quad (3)$$

where y is the percentage of enzyme activity, live parasites or live cells in IC_{50}, EC_{50} and CC_{50} determinations, respectively, x is the inhibitor/drug concentration, and s is the slope factor (also called Hill slope) that quantifies the steepness of the dose-response curve.

The reciprocal value of the initial reaction rates of *Li*TryS ligase reaction progress curves at different compound (**1** or **3**) and substrate (ATP or GspdSH) concentrations were fitted to the reciprocal equation that describes competitive inhibition [42]:

$$\frac{1}{v} = \frac{1}{V_{max}} + \left(\frac{1}{[S]}\frac{K_m}{V_{max}}\right)\left(1 + \frac{[I]}{K_i}\right) \quad (4)$$

The reciprocal value of the initial reaction rates of *Li*TryS ligase reaction progress curves at different compound **4** and GspdSH concentrations were fitted to the reciprocal equation that describes hyperbolic noncompetitive inhibition [43]:

$$\frac{1}{v} = \frac{1}{V_{max}}\left(\frac{\alpha K_i + [I]}{\alpha K_i + \beta[I]}\right) + \frac{\alpha K_m}{V_{max}}\left(\frac{K_i + [I]}{\alpha K_i + \beta[I]}\right)\frac{1}{[S]} \quad (5)$$

4.3. Computational methods

The molecular graphics program PyMOL (Schrodinger, L. L. C. The PyMOL Molecular Graphics System, v. 1.8, 2015) was employed for molecular editing, visualization, and figure preparation.

4.3.1. Protein model building

Entries 2VPS, 2VPM, and 2VOB reporting three crystallographic forms of the apo form of *Lm*TryS [15] were retrieved from the Protein Data Bank (PDB) [44]. To complete the Gly250–Val262 stretch, which was not visible in these X-ray crystal structures, and to introduce the necessary amino acid substitutions to create a model of the ligase domain of *Li*TryS, we used the Robetta server [45] and the sequence from Uniprot entry A4I2Z3. We also made use of several crystal structures of *Ec*GspS in the apo open state and in the closed state in complex with nucleotides, GSH and a phosphinate inhibitor (PDB ids.: 2IOA, 2IOB, 2IO7, 2IO8, and 2IO9) [29] as templates for model building using the SWISS-MODEL server [46]. All the models were visually inspected and corrected to avoid steric clashes. The final consensus working model comprised residues 217–633.

4.3.2. Ligand preparation

Molecular models of free GSH and Spd were retrieved from PDB entries 1AQW [47] and 1POT [37], respectively. The starting structures for GspdSH (GSP) and the transition state of the reaction (TS) were modeled interactively using PyMOL and ligand GGA from PDB entry 2IOA [29] as the template. Geometry optimization of all of these ligands and point charge derivation were achieved by means of the AM1-BCC hamiltonian available in the *sqm* program [48] and use was made of the *peptide_corr = 1* keyword for GSH and GSP. The generalized AMBER force field (gaff) [49] was used for ligand atoms. Standard geometries and connectivities for cofactors ATP and ADP, containing standard AMBER parameters and optimized point charges for phosphates [50], were retrieved from the AMBER database (http://amber.manchester.ac.uk/). The binding pose for ATP was assumed to resemble that of

β,γ-imidoadenosine 5′-triphosphate (AMP-PNP) in complex with *Ec*GspS (PDB id. 2IO7) [29].

4.3.3. Energy minimization and molecular dynamics simulations

The *leaprcff14SB* AMBER force field and the graphics processing unit (GPU)-based implementation of the *pmemd.cuda* module of AMBER18 in the single-precision−fixed-precision (SPFP) mode were used, as described before [23]. To reduce the artifactually strong attraction of Mg^{2+} ions by the nucleotide phosphate oxygens, an r^{-4} term that takes into account the ion-induced dipole interaction was added to the 12-6 Lennard-Jones model [51].

4.3.4. Automated ligand docking

A three-dimensional cubic grid encompassing the whole protein with a spacing of 0.375 Å centered at the *Li*TryS active site was defined for ligand docking. AutoDock Vina 1.2 [52] was used to generate up to 10 feasible binding poses for each ligand studied. The best poses were ranked on the basis of results from intra- and intermolecular energy evaluations.

Declaration of competing interest

The authors declare that they have no known competing financial interests or personal relationships that could have appeared to influence the work reported in this paper.

Data availability

Data will be made available on request.

Acknowledgements

This work has been supported by the Spanish MICINN (Projects PID2019-104070RB-C21 and PID2019-104070RBC22), the Spanish National Research Council (CSIC, Projects CSIC-PIE-201980E100 and CSIC-PIE-201980E028), and the Comunidad de Madrid (PLATESA2-CM ref S-2018/BAA-4370). The MCIN is also acknowledged for the pre-doctoral fellowship to M.A.C.

Appendix A. Supplementary data

Supplementary data to this article can be found online at https://doi.org/10.1016/j.ejmech.2022.114675.

References

[1] Leishmaniasis, in, World Health Organization, 2022.
[2] G.D. Melo, S. Goyard, L. Fiette, A. Boissonnas, C. Combadiere, G.F. Machado, P. Minoprio, T. Lang, Unveiling Cerebral Leishmaniasis: parasites and brain inflammation in *Leishmania donovani* infected mice, Sci. Rep. 7 (2017) 8454, https://doi.org/10.1038/s41598-017-09085-5.
[3] V. Lievin-Le Moal, P.M. Loiseau, *Leishmania* hijacking of the macrophage intracellular compartments, FEBS J. 283 (2016) 598–607, https://doi.org/10.1111/febs.13601.
[4] L. Van Bockstal, S. Hendrickx, L. Maes, G. Caljon, Sand fly studies predict transmission potential of drug-resistant *Leishmania*, Trends Parasitol. 36 (2020) 785–795, https://doi.org/10.1016/j.pt.2020.06.006.
[5] J.A. Brannigan, A.J. Wilkinson, Drug discovery in leishmaniasis using protein lipidation as a target, Biophysical Reviews 13 (2021) 1139–1146, https://doi.org/10.1007/s12551-021-00855-0.
[6] P. Mazire, V. Agarwal, A. Roy, Road-map of pre-clinical treatment for visceral leishmaniasis, Drug Dev. Res. 83 (2022) 317–327, https://doi.org/10.1002/ddr.21907.
[7] Leishmaniasis, in, World Health Organization.
[8] P.M. Gillespie, C.M. Beaumier, U. Strych, T. Hayward, P.J. Hotez, M.E. Bottazzi, Status of vaccine research and development of vaccines for leishmaniasis, Vaccine 34 (2016) 2992–2995, https://doi.org/10.1016/j.vaccine.2015.12.071.
[9] Visceral leishmaniasis, in, Drug for Neglected Diseases Initiatitive.
[10] A.A. Bekhit, E. El-Agroudy, A. Helmy, T.M. Ibrahim, A. Shavandi, A.E.A. Bekhit, *Leishmania* treatment and prevention: natural and synthesized drugs, Eur. J. Med. Chem. 160 (2018) 229–244, https://doi.org/10.1016/j.ejmech.2018.10.022.
[11] S. Hendrickx, G. Caljon, L. Maes, Need for sustainable approaches in antileishmanial drug discovery, Parasitol. Res. 118 (2019) 2743–2752, https://doi.org/10.1007/s00436-019-06443-2.
[12] L.S. Torrie, S. Wyllie, D. Spinks, S.L. Oza, S. Thompson, J.R. Harrison, I.H. Gilbert, P.G. Wyatt, A.H. Fairlamb, J.A. Frearson, Chemical validation of trypanothione synthetase: a potential drug target for human trypanosomiasis, J. Biol. Chem. 284 (2009) 36137–36145, https://doi.org/10.1074/jbc.M109.045336.
[13] S. Wyllie, S.L. Oza, S. Patterson, D. Spinks, S. Thompson, A.H. Fairlamb, Dissecting the essentiality of the bifunctional trypanothione synthetase-amidase in *Trypanosoma brucei* using chemical and genetic methods, Mol. Microbiol. 74 (2009) 529–540, https://doi.org/10.1111/j.1365-2958.2009.06761.x.
[14] R.L. Krauth-Siegel, M.A. Comini, Redox control in trypanosomatids, parasitic protozoa with trypanothione-based thiol metabolism, Biochim. Biophys. Acta 1780 (2008) 1236–1248, https://doi.org/10.1016/j.bbagen.2008.03.006.
[15] P.K. Fyfe, S.L. Oza, A.H. Fairlamb, W.N. Hunter, *Leishmania* trypanothione synthetase-amidase structure reveals a basis for regulation of conflicting synthetic and hydrolytic activities, J. Biol. Chem. 283 (2008) 17672–17680, https://doi.org/10.1074/jbc.M801850200.
[16] A.F. Sousa, A.G. Gomes-Alves, D. Benitez, M.A. Comini, L. Flohe, T. Jaeger, J. Passos, F. Stuhlmann, A.M. Tomas, H. Castro, Genetic and chemical analyses reveal that trypanothione synthetase but not glutathionylspermidine synthetase is essential for *Leishmania infantum*, Free Radic. Biol. Med. 73 (2014) 229–238, https://doi.org/10.1016/j.freeradbiomed.2014.05.007.
[17] D. Benitez, A. Medeiros, L. Fiestas, E.A. Panozzo-Zenere, F. Maiwald, K.C. Prousis, M. Roussaki, T. Calogeropoulou, A. Detsi, T. Jaeger, J. Sarlauskas, L. Peterlin Masic, C. Kunick, G.R. Labadie, L. Flohe, M.A. Comini, Identification of novel chemical scaffolds inhibiting trypanothione synthetase from pathogenic trypanosomatids, PLoS Neglected Trop. Dis. 10 (2016), e0004617, https://doi.org/10.1371/journal.pntd.0004617.
[18] A. Medeiros, D. Benitez, R.S. Korn, V.C. Ferreira, E. Barrera, F. Carrion, O. Pritsch, S. Pantano, C. Kunick, C.I. de Oliveira, O.C.F. Orban, M.A. Comini, Mechanistic and biological characterisation of novel N(5)-substituted paullones targeting the biosynthesis of trypanothione in *Leishmania*, J. Enzym. Inhib. Med. Chem. 35 (2020) 1345–1358, https://doi.org/10.1080/14756366.2020.1780227.
[19] P. Saudagar, V.K. Dubey, Cloning, expression, characterization and inhibition studies on trypanothione synthetase, a drug target enzyme, from *Leishmania donovani*, Biol. Chem. 392 (2011) 1113–1122, https://doi.org/10.1515/BC.2011.222.
[20] P. Saudagar, P. Saha, A.K. Saikia, V.K. Dubey, Molecular mechanism underlying antileishmanial effect of oxabicyclo[3.3.1]nonanones: inhibition of key redox enzymes of the pathogen, Eur. J. Pharm. Biopharm. 85 (2013) 569–577, https://doi.org/10.1016/j.ejpb.2013.08.014.
[21] D. Benitez, J. Franco, F. Sardi, A. Leyva, R. Duran, G. Choi, G. Yang, T. Kim, N. Kim, J. Heo, K. Kim, H. Lee, I. Choi, C. Radu, D. Shum, J.H. No, M.A. Comini, Drug-like molecules with anti-trypanothione synthetase activity identified by high throughput screening, J. Enzym. Inhib. Med. Chem. 37 (2022) 912–929, https://doi.org/10.1080/14756366.2022.2045590.
[22] S. Zimmermann, M. Oufir, A. Leroux, R.L. Krauth-Siegel, K. Becker, M. Kaiser, R. Brun, M. Hamburger, M. Adams, Cynaropicrin targets the trypanothione redox system in *Trypanosoma brucei*, Bioorg. Med. Chem. 21 (2013) 7202–7209, https://doi.org/10.1016/j.bmc.2013.08.052.
[23] A. Revuelto, H. de Lucio, J.C. García-Soriano, P.A. Sánchez-Murcia, F. Gago, A. Jiménez-Ruiz, M.-J. Camarasa, S. Velázquez, Efficient dimerization disruption of *Leishmania infantum* trypanothione reductase by triazole-phenyl-thiazoles, J. Med. Chem. 64 (2021) 6137–6160, https://doi.org/10.1021/acs.jmedchem.1c00206.
[24] G.D. E, P. Carrero, A. Madrona, P. Rodriguez-Salamanca, B. Martinez-Gualda, M. J. Camarasa, M.L. Jimeno, P.R. Bennallack, J.G. Finnell, T.M. Tsang, K. A. Christensen, A. San-Felix, M.S. Rogers, Galloyl carbohydrates with antiangiogenic activity mediated by capillary morphogenesis gene 2 (CMG2) protein binding, J. Med. Chem. 62 (2019) 3958–3970, https://doi.org/10.1021/acs.jmedchem.8b01988.
[25] A. Jimenez, P. Garcia, S. de la Puente, A. Madrona, M.J. Camarasa, M.J. Perez-Perez, J.C. Quintela, F. Garcia-Del Portillo, A. San-Felix, A novel class of cationic and non-peptidic small molecules as hits for the development of antimicrobial agents, Molecules 23 (2018), https://doi.org/10.3390/molecules23071513.
[26] M. Piazza, C. Rossini, S. Della Fiorentina, C. Pozzi, F. Comelli, I. Bettoni, P. Fusi, B. Costa, F. Peri, Glycolipids and benzylammonium lipids as novel antisepsis agents: synthesis and biological characterization, J. Med. Chem. 52 (2009) 1209–1213, https://doi.org/10.1021/jm801333m.
[27] S.L. Croft, D. Snowdon, V. Yardley, The activities of four anticancer alkyllysophospholipids against Leishmania donovani, Trypanosoma cruzi and Trypanosoma brucei, J. Antimicrob. Chemother. 38 (1996) 1041–1047, https://doi.org/10.1093/jac/38.6.1041.
[28] A.G. Murzin, Structural classification of proteins: new superfamilies, Curr. Opin. Struct. Biol. 6 (1996) 386–394, https://doi.org/10.1016/S0959-440X(96)80059-5.
[29] C.H. Pai, B.Y. Chiang, T.P. Ko, C.C. Chou, C.M. Chong, F.J. Yen, S. Chen, J. K. Coward, A.H. Wang, C.H. Lin, Dual binding sites for translocation catalysis by Escherichia coli glutathionylspermidine synthetase, EMBO J. 25 (2006) 5970–5982, https://doi.org/10.1038/sj.emboj.7601440.
[30] A.E. Leroux, J.R. Haanstra, B.M. Bakker, R.L. Krauth-Siegel, Dissecting the catalytic mechanism of Trypanosoma brucei trypanothione synthetase by kinetic analysis and computational modeling, J. Biol. Chem. 288 (2013) 23751–23764, https://doi.org/10.1074/jbc.M113.483289.
[31] J.A. Bueren-Calabuig, C. Coderch, E. Rico, A. Jimenez-Ruiz, F. Gago, Mechanistic insight into the catalytic activity of betabetaalpha-metallonucleases from computer

simulations: Vibrio vulnificus periplasmic nuclease as a test case, Chembiochem 12 (2011) 2615–2622, https://doi.org/10.1002/cbic.201100485.
[32] C. Coderch, E. Lence, A. Peon, H. Lamb, A.R. Hawkins, F. Gago, C. Gonzalez-Bello, Mechanistic insight into the reaction catalysed by bacterial type II dehydroquinases, Biochem. J. 458 (2014) 547–557, https://doi.org/10.1042/BJ20131103.
[33] A. Negri, E. Marco, J. Damborsky, F. Gago, Stepwise dissection and visualization of the catalytic mechanism of haloalkane dehalogenase LinB using molecular dynamics simulations and computer graphics, J. Mol. Graph. Model. 26 (2007) 643–651, https://doi.org/10.1016/j.jmgm.2007.03.010.
[34] O. Koch, D. Cappel, M. Nocker, T. Jager, L. Flohe, C.A. Sotriffer, P.M. Selzer, Molecular dynamics reveal binding mode of glutathionylspermidine by trypanothione synthetase, PLoS One 8 (2013), e56788, https://doi.org/10.1371/journal.pone.0056788.
[35] M. Comini, U. Menge, J. Wissing, L. Flohe, Trypanothione synthesis in crithidia revisited, J. Biol. Chem. 280 (2005) 6850–6860, https://doi.org/10.1074/jbc.M404486200.
[36] J.B. Thoden, H.M. Holden, S.M. Firestine, Structural analysis of the active site geometry of N5-carboxyaminoimidazole ribonucleotide synthetase from Escherichia coli, Biochemistry 47 (2008) 13346–13353, https://doi.org/10.1021/bi801734z.
[37] S. Sugiyama, Y. Matsuo, K. Maenaka, D.G. Vassylyev, M. Matsushima, K. Kashiwagi, K. Igarashi, K. Morikawa, The 1.8-A X-ray structure of the Escherichia coli PotD protein complexed with spermidine and the mechanism of polyamine binding, Protein Sci. 5 (1996) 1984–1990, https://doi.org/10.1002/pro.5560051004.
[38] S.L. Oza, E. Tetaud, M.R. Ariyanayagam, S.S. Warnon, A.H. Fairlamb, A single enzyme catalyses formation of Trypanothione from glutathione and spermidine in Trypanosoma cruzi, J. Biol. Chem. 277 (2002) 35853–35861, https://doi.org/10.1074/jbc.m204403200.
[39] S.L. Oza, M.P. Shaw, S. Wyllie, A.H. Fairlamb, Trypanothione biosynthesis in Leishmania major, Mol. Biochem. Parasitol. 139 (2005) 107–116, https://doi.org/10.1016/j.molbiopara.2004.10.004.
[40] M. De Rycker, I. Hallyburton, J. Thomas, L. Campbell, S. Wyllie, D. Joshi, S. Cameron, I.H. Gilbert, P.G. Wyatt, J.A. Frearson, A.H. Fairlamb, D.W. Gray, Comparison of a high-throughput high-content intracellular Leishmania donovani assay with an axenic amastigote assay, Antimicrob. Agents Chemother. 57 (2013) 2913–2922, https://doi.org/10.1128/AAC.02398-12.
[41] J. Inglese, R.L. Johnson, A. Simeonov, M. Xia, W. Zheng, C.P. Austin, D.S. Auld, High-throughput screening assays for the identification of chemical probes, Nat. Chem. Biol. 3 (2007) 466–479, https://doi.org/10.1038/nchembio.2007.17.
[42] R.A. Copeland, Enzymes, A Practical Introduction to Structure, Mechanism, and Data Analysis, Wiley-VCH, 2000.
[43] V. Leskovac, Comprehensive Enzyme Kinetics, Springer, 2003.
[44] H.M. Berman, J. Westbrook, Z. Feng, G. Gilliland, T.N. Bhat, H. Weissig, I. N. Shindyalov, P.E. Bourne, The protein Data Bank, Nucleic Acids Res. 28 (2000) 235–242, https://doi.org/10.1093/nar/28.1.235.
[45] D.E. Kim, D. Chivian, D. Baker, Protein structure prediction and analysis using the Robetta server, Nucleic Acids Res. 32 (2004) W526–W531, https://doi.org/10.1093/nar/gkh468.
[46] A. Waterhouse, M. Bertoni, S. Bienert, G. Studer, G. Tauriello, R. Gumienny, F. T. Heer, T.A.P. de Beer, C. Rempfer, L. Bordoli, R. Lepore, T. Schwede, SWISS-MODEL: homology modelling of protein structures and complexes, Nucleic Acids Res. 46 (2018) W296–W303, https://doi.org/10.1093/nar/gky427.
[47] L. Prade, R. Huber, T.H. Manoharan, W.E. Fahl, W. Reuter, Structures of class pi glutathione S-transferase from human placenta in complex with substrate, transition-state analogue and inhibitor, Structure 5 (1997) 1287–1295, https://doi.org/10.1016/S0969-2126(97)00281-5.
[48] R.C. Walker, M.F. Crowley, D.A. Case, The implementation of a fast and accurate QM/MM potential method in Amber, J. Comput. Chem. 29 (2008) 1019–1031, https://doi.org/10.1002/jcc.20857.
[49] J. Wang, R.M. Wolf, J.W. Caldwell, P.A. Kollman, D.A. Case, Development and testing of a general amber force field, J. Comput. Chem. 25 (2004) 1157–1174, https://doi.org/10.1002/jcc.20035.
[50] K.L. Meagher, L.T. Redman, H.A. Carlson, Development of polyphosphate parameters for use with the AMBER force field, J. Comput. Chem. 24 (2003) 1016–1025, https://doi.org/10.1002/jcc.10262.
[51] P. Li, K.M. Merz Jr., Taking into account the ion-induced dipole interaction in the nonbonded model of ions, J. Chem. Theor. Comput. 10 (2014) 289–297, https://doi.org/10.1021/ct400751u.
[52] J. Eberhardt, D. Santos-Martins, A.F. Tillack, S. Forli, AutoDock Vina 1.2.0: new docking methods, expanded force field, and Python bindings, J. Chem. Inf. Model. 61 (2021) 3891–3898, https://doi.org/10.1021/acs.jcim.1c00203.